Reconfigurable RF MEMS Phased Array Antenna Integrated Within a Liquid Crystal Polymer (LCP) System-on-Package

Nickolas Kingsley, *Member, IEEE*, George E. Ponchak, *Senior Member, IEEE*, and John Papapolymerou, *Senior Member, IEEE*

***Abstract*—For the first time, a fully integrated phased array antenna with radio frequency microelectromechanical systems (RF MEMS) switches on a flexible, organic substrate is demonstrated above 10 GHz. A low noise amplifier (LNA), MEMS phase shifter, and 2×2 patch antenna array are integrated into a system-on-package (SOP) on a liquid crystal polymer substrate. Two antenna arrays are compared; one implemented using a single-layer SOP and the second with a multilayer SOP. Both implementations are low-loss and capable of 12° of beam steering. The design frequency is 14 GHz and the measured return loss is greater than 12 dB for both implementations. The use of an LNA allows for a much higher radiated power level. These antennas can be customized to meet almost any size, frequency, and performance needed. This research furthers the state-of-the-art for organic SOP devices.**

***Index Terms*—Beam steering, flexible, liquid crystal polymer (LCP), low noise amplifier (LNA), multilayer, organic, phase shifter, phased array antenna, radio frequency microelectromechanical systems (RF MEMS), system-on-package (SOP).**

I. Introduction

PHASED ARRAY antennas are critical components for automobile collision avoidance radar, military radar, and space communication systems. The antenna system requires the integration of several components such as amplifiers, phase shifters, and RF power distribution networks. Costs can be decreased by using microwave monolithic integrated circuits (MMICs) for the amplifiers and phase shifters because they use standard integrated circuit processing. Lately, radio frequency microelectromechanical systems (RF MEMS) phase shifters have been demonstrated with lower insertion loss [1], which makes them a better alternative to MMIC phase shifters. However, practical implementation of phased array antennas with MMICs and RF MEMS phase shifters have been hampered by the high cost of packaging and integration [2], [3]. Flexible phased arrays that may be rolled for storage and delivery and unrolled for use is especially difficult using standard packaging technology. To offer greater functionality in a smaller volume, RF systems are moving towards a system-on-package (SOP) approach. SOP technologies are widely desired for their design simplicity, lower cost, higher system function integration, better electrical performance, and various 3D packaging capabilities [4]. For example, a variety of components (passive, active, electromechanical, optical, etc.) can be integrated into one packaged system to reduce the size, improve the performance, and lower the cost.

When designing an SOP, the substrate and packaging material must be carefully considered. Semiconductor SOPs have been demonstrated and have the advantage of using a mature fabrication technology and permitting the monolithic integration of some electronic components on the semiconductor substrates [5], but they are fragile, limited to small sizes, and not suitable for flexible antenna arrays. Low temperature cofired ceramic (LTCC) is the most widely used material for microwave SOP systems [6]. It is hermetic, stable over a wide range of temperatures, and has low dielectric losses. However, like semiconductors, LTCC is not suitable for flexible antenna arrays, and it requires high temperature processes that are not suitable for RF MEMS circuits.

Organic materials such as Duroid [7] and FR-4 [8] have been explored for use with SOP applications. They are both very low-cost materials and have low loss up to about 10 GHz, but to date, a low-cost, reliable method for making MEMS switches on these materials has not been demonstrated. LCP is a unique material for SOP applications. It is low-cost, has low dielectric loss (to well over 100 GHz [9]), is flexible, and it can be fabricated in large panels or on long rolls. Moreover, reliable RF MEMS circuits can be fabricated directly on the material [10].

In this paper, a 14 GHz phased array antenna for use in a NASA Earth observing satellite system packaged using system-on-package technology and LCP is demonstrated for the first time. The fully-integrated array consists of a MMIC LNA, MEMS phase shifter, RF power distribution network, biasing circuits, and antenna array. In the following sections, the phased array system, the fabrication procedures, the measurement system, and the measured results are described and compared to simulated results.

II. Phased Array SOP Description

The schematic for a receive-mode phased array antenna system is shown in Fig. 1. An MMIC low noise amplifier (LNA) provides signal amplification and is ideally suited for

Manuscript received May 1, 2007; revised August 8, 2007. This work was supported in part by NASA under Contract NNG05GP93G and in part by Raytheon.

N. Kingsley was with the School of Electrical and Computer Engineering, Georgia Institute of Technology, Atlanta, GA 30308 USA. He is now with Auriga Measurement Systems, Lowell, MA 01854 USA (e-mail: kingsley@gatech.edu).

G. E. Ponchak is with the NASA Glenn Research Center, Cleveland, OH 44135 USA.

J. Papapolymerou is with the School of Electrical and Computer Engineering, Georgia Institute of Technology, Atlanta, GA 30308 USA.

Digital Object Identifier 10.1109/TAP.2007.913151

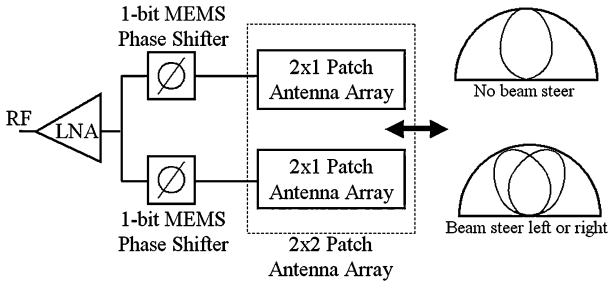

Fig. 1. Block diagram for a receive-mode phased array antenna is shown.

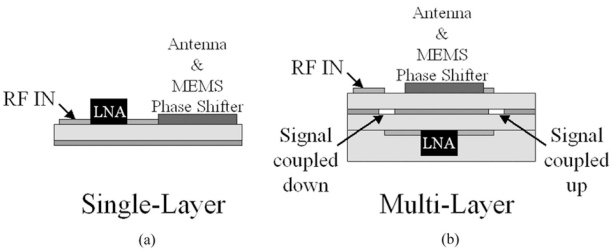

Fig. 2. Side view comparison of single and multilayer implementations of the antenna arrays. The multilayer implementation uses the same components as the single-layer implementation but it is smaller in size.

a receiver front end. Microstrip T-junctions are used with impedance matching sections to split the signal throughout the feed network. A pair of one-bit RF MEMS phase shifters are fabricated monolithically onto the LCP to provide beam steering. Microstrip patch antennas are used to receive the radiated signal.

The phased array antenna is packaged in two different SOPs to demonstrate the functionality of LCP for this application. First, a single-layer SOP is implemented as shown in Fig. 2(a), and then a multilayer SOP is implemented as shown in Fig. 2(b). The single-layer SOP has the advantages of low cost, easy fabrication, and it permits rework of the system because all of the components are visible. However, because RF and dc bias lines cannot easily cross, the single-layer SOP is larger, and as functionality is increased, single-layer SOPs may be of limited use. The multilayer implementation is more challenging to design and fabricate and it does not permit rework, but the overall size can be kept small, and more functionality can be added by increasing the thickness and keeping the footprint size constant. In addition, the multilayer SOP may have higher loss due to radiation from the vertical interconnects that are required. The procedure that was used to design, fabricate, and test these modules is presented in this paper.

III. Component Design

Before the phased array antenna could be assembled, each component must be individually designed and optimized. The four main components of the phased array antenna are: the patch antenna array; the phase shifter; the RF power distribution network, which includes the impedance matched T-junctions and the apertures for vertical power transition in the multilayer SOP, and the LNA.

TABLE I
Patch Antenna Dimensions Calculated Using Equations Given in [11]

Parameter	Calculated Value
W	7.620mm
ε_{reff}	2.881
ΔL	49.616μm
L	6.209mm

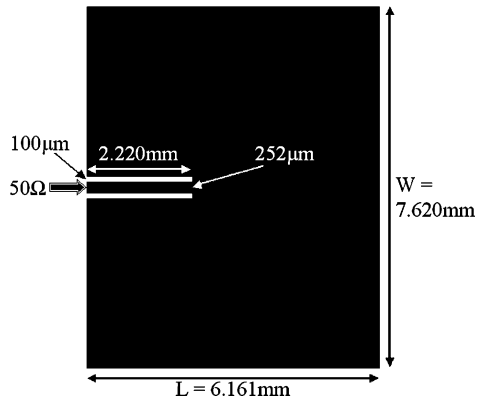

Fig. 3. Final patch antenna geometry optimized using a full-wave simulator to resonate at 14 GHz with a 50 Ω input impedance.

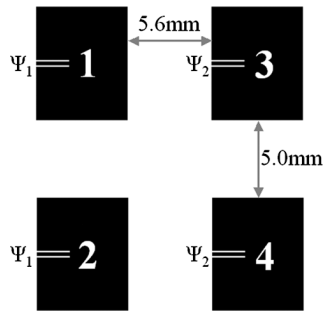

Fig. 4. 2×2 antenna array layout. Patches 1 and 2 are fed with phase Ψ_1 and patches 3 and 4 are fed with phase Ψ_2. The signal amplitude is the same to all four patches.

A. Patch Antenna Array Design

To create the patch antenna array, a single patch is designed and then expanded to a 2×2 array.

1) Single Patch Design: The antenna geometry was designed using equations given in [11] for patch antennas. Table I shows these values for 100 μm thick LCP with an ε_r of 2.95. W is the width of the patch, $\varepsilon_{\text{reff}}$ is the effective dielectric constant, ΔL is the patch extension length, and L is the final patch length.

The geometry suggested by Table I was entered into an ADS Momentum simulation. The length was tuned to resonate at 14.0 GHz. The recessed microstrip feed length was increased until an input impedance of 50 Ω was achieved. The final layout with dimensions is shown in Fig. 3. Simulations show the single patch antenna has a directive gain of 6.94 dBi at 14 GHz.

2) 2×2 Patch Array: The 2×2 patch array was designed to minimize the distance between the patches, which minimizes the array size and the side lobe level. The 2×2 patch antenna array is shown in Fig. 4. Patches 1 and 2 are fed with phase Ψ_1

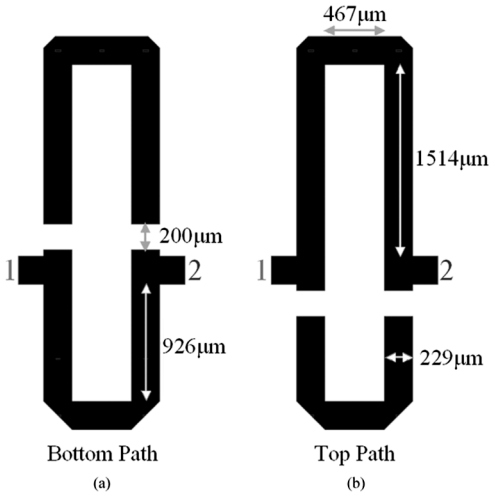

Fig. 5. Layout of 1-bit phase shifter with all dimensions labeled. The gaps denote the location of the MEMS switches. Signal propagates through the: (a) bottom path and (b) top path.

and patches 3 and 4 are fed with phase Ψ_2. If Ψ_1 and Ψ_2 are the same then the antenna radiates perpendicular to the substrate. If they are not the same then the beam is steered left or right. The signal amplitude is the same to all four patches.

As the number of elements is doubled, an additional 3 dB of directive gain is expected and with four radiating elements an additional 6 dB is expected. Since the simulated directivity increased from 6.94 dB for the single patch to 12.49 dB for the 2×2 array, this was confirmed.

B. Phase Shifter Design

There is a correlation between phase shift, degree of beam steering, and the side lobe level. The four patches can be fed independently using the ADS Momentum software. This correlation was explored by varying the phase shift to the patches in Fig. 4 (Ψ_1 and Ψ_2) and recording the degree of beam steering and the side lobe level. As the phase shift is increased, the amount of beam steering increases but the side lobe level also increases. To implement the maximum amount of beam steering while maintaining a low side lobe level (15 dB or better), a phase shift of 30° is required.

RF MEMS switched line phase shifters on LCP have been previously demonstrated [1]. The wavelength of a microstrip line on 100 μm thick LCP at 14 GHz is approximately 13.9 mm. In order to get the desired phase shift, a length difference of $30°/360°$ or 1/12th of a wavelength (1.16 mm) is needed between the two paths. The design was optimized using Momentum and the final layout is shown in Fig. 5. When the bottom two MEMS switches are activated, the signal propagates through the bottom path [Fig. 5(a)]. When the top two MEMS switches are activated, the signal propagates through the top path [Fig. 5(b)].

The gaps in this figure denote the location of the RF MEMS switches. These switches have an on-state insertion loss of 0.20 dB at the design frequency. They have an off-state isolation of more than 30 dB. The activation time for these switches is 40 μs or less [10].

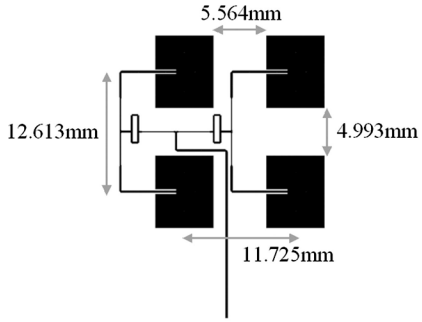

Fig. 6. Final 2×2 antenna array layout with phase shifters and RF power distribution network is shown.

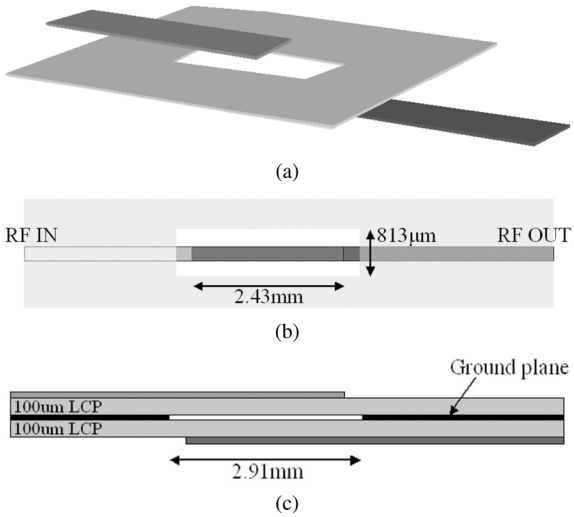

Fig. 7. Layout of aperture coupling component from the (a) perspective, (b) top, and (c) side views. All important dimensions are labeled.

C. RF Power Distribution Network Design

The layout of the patch array, phase shifters, and RF power distribution network is shown in Fig. 6. The distance between the patches is given in this figure.

RF power is distributed to the four patch antennas by a series of microstrip lines. The input signal is split twice at T-junctions before reaching the patches. Since each patch must receive the same power level for proper operation, symmetry is maintained after the first T-junction. Quarter-wave transformers are used to maintain a 50 Ω impedance throughout the feed network.

To implement a multilayer device, the RF signal needs to be coupled between transmission lines on different layers. This is usually done using metalized vias or aperture coupling. Wide frequency bandwidth, vertical via hole interconnects have been demonstrated on LCP [12], but they require extra processing steps and cost. Microstrip patch antenna elements are narrow bandwidth, and the vertical interconnects required for this array must pass through the ground plane. Thus, aperture coupling was chosen here as shown in Fig. 7. Design guidelines for aperture coupling slots were published in [13]. The slot dimensions should be kept as small as possible while maintaining a good impedance match and the amount of overlap between the signal lines determines the resonant frequency of the aperture (the resonant frequency is inversely proportional to the length of the

TABLE II
OPTIMIZED DIMENSIONS FOR APERTURE COUPLING ON 100 μm THICK LCP

Dimension	Length	Length (wavelength)
Slot width	813μm	$^1/_{18}\lambda$
Slot length	2.91mm	$^1/_5\lambda$
Overlap length	2.43mm	$^1/_6\lambda$

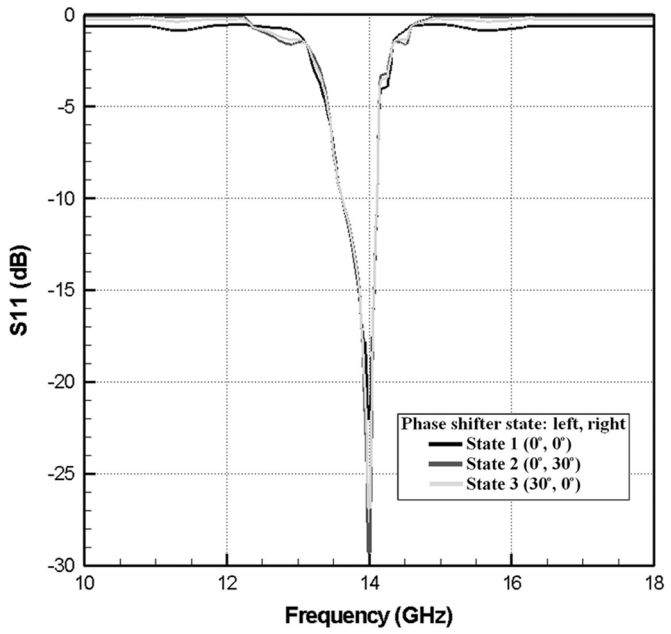

Fig. 8. Simulated return loss for the 2 × 2 antenna array with phase shifters is shown. The geometry was shown in Fig. 6.

overlap). ADS Momentum was used to optimize the slot dimensions and overlap length. These values are given in Table II, and the final design is shown in Fig. 7. ADS predicted an insertion loss less than 0.25 dB at 14 GHz.

D. Phased Array Design

To implement the beam steering, the phase shifters can be set to one of three states.

1) Both phases can be the same (either 0° or 30°)—Beam is not steered;
2) The left phase shifter is 0° and the right phase shifter is 30°—Beam is steered left ($-\theta$ direction);
3) The left phase shifter is 30° and the right phase shifter is 0°—Beam is steered right ($+\theta$ direction).

The simulated S11 for these three states is shown in Fig. 8 and the simulated radiation patterns are shown in Fig. 9. The simulated side lobe levels are more than 10 dB lower than the main lobe. The simulated directivity and angle of maximum radiation are given in Table III.

Symmetry is maintained in regards to the signal line length to each patch. This is necessary for proper array feeding. However, the feed is clearly not located in the center of the antenna (as shown in Fig. 6). The feed is centered towards the left side of the antenna (between patches 1 and 2 from Fig. 4). This has a slight influence on the direction of radiation and causes the degree of beam steering to be non-symmetric.

The degree of beam steering is detailed in Fig. 10.

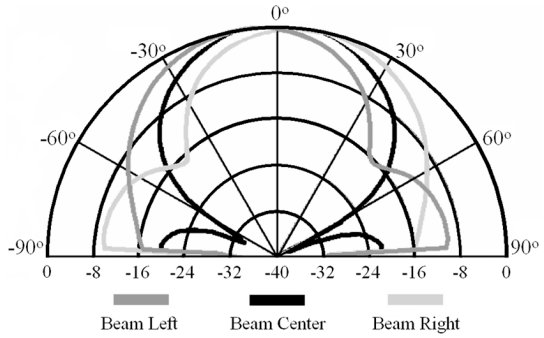

Fig. 9. Simulated patterns for the 2 × 2 antenna array with phase shifters. The geometry was shown in Fig. 6. All cuts are taken in the $\phi = 0°$ (E-co) plane.

TABLE III
SIMULATED DIRECTIVITY AND ANGLE OF MAXIMUM RADIATION IS GIVEN

State	Simulated Directivity	Angle of maximum radiation (θ)
1 (center)	12.58 dB	0.00^o
2 (left)	12.22 dB	-9.00^o
3 (right)	12.18 dB	6.00^o

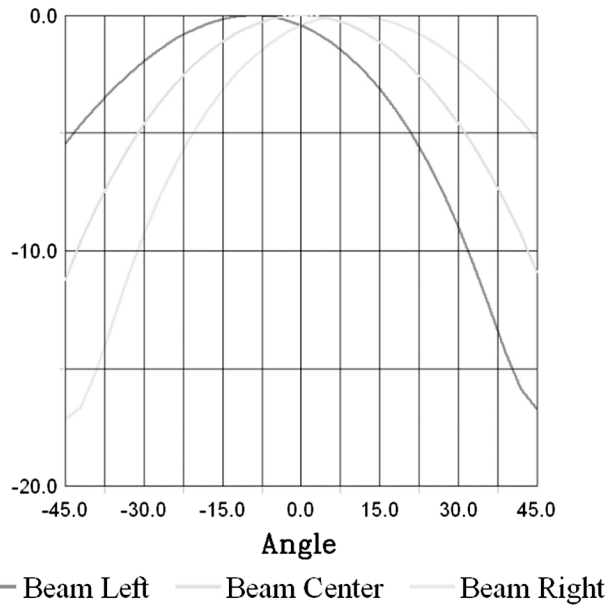

Fig. 10. Degree of beam steering from Fig. 9 is shown. The total amount of beam steering is 15°.

E. LNA Design

To provide amplification of the RF signal, a 30 dB, *Ku*-band low-noise amplifier (LNA) from Raytheon RF Components was used. Since this LNA was designed using microwave transmission lines to work at 50 Ω, no additional matching networks were needed. To prevent oscillation, 100 pF and a 10 000 pF off-chip capacitors were added in series between the dc bias and ground pads. These values were recommended by the chip designers. The chip can be driven with up to 2.5 V and 66 mA of dc current.

IV. SYSTEM-ON-PACKAGE INTEGRATION

Phased array antennas integrated within single and multilayer system-on-packages were designed and fabricated.

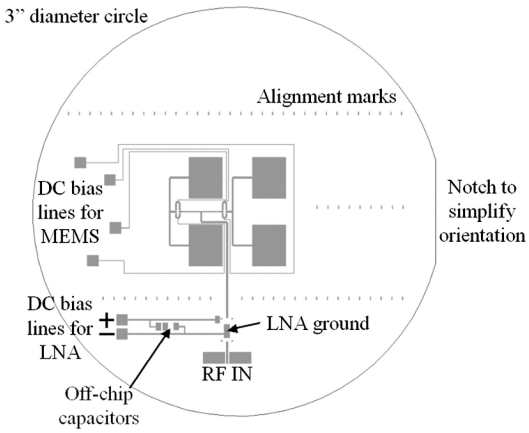

Fig. 11. Layout of single-layer antenna array. The 2 × 2 patch antenna array, MEMS phase shifters, bias lines, and LNA pads are shown.

A. Single-Layer System-On-Package

The layout of the single-layer implementation is shown in Fig. 11. The size of the layout could be reduced by moving around the placement of the dc bias lines and LNA. The antenna array is fabricated on a 3 inch diameter circle that is precisely cut using a CO_2 laser. This diameter was used because it is the largest size that can be exposed in the chosen mask aligner. The thickness of the LCP is 100 μm. A notch is etched on one side which helps keep the device aligned during fabrication. The circular shape was chosen because it tends to have fewer issues with surface wave edge effects.

The sample was polished before processing to provide a smooth surface for MEMS fabrication. An electron beam evaporator was used to deposit a 200A-2000Å Ti-Au layer. A 2000Å silicon nitride layer was deposited using PECVD and etched using an RIE. A 2 μm thick sacrificial photoresist layer was patterned and hard baked. An electron beam evaporator was used again to deposit a 200A-2000A-200A Ti-Au-Ti layer. Electroplating was used to increase the gold thickness of the antennas and MEMS bridges to 1.5 μm. The sacrificial photoresist layer was removed using a stripping agent and dried with a CO_2 critical point dryer. All processing steps were kept below 150°C and line width tolerances were within 3 μm of the desired value.

The dc bias lines for the capacitive RF MEMS switches were evaporated with the first seed layer and were not plated. With a width of 15 μm and a thickness of 2000 Å, these lines have very high impedance which reduces the amount of RF energy that propagates down the dc path.

The ground and bias pads for integration of the MMIC LNA were added at the same time as the MEMS to prevent any additional process steps. Once the MEMS were released, the LNA and off-chip capacitors were mounted onto the sample using silver epoxy. Alignment marks were added to help place the chip squarely between the signal lines. The epoxy was cured for 2 hours at 100°C to harden the connection and increase the conductivity of the epoxy. Finally, wire bonds were added to connect the LNA to the dc bias and RF signal lines. The placement of the wire bonds is shown in Fig. 12. The fabricated single-layer SOP antenna is shown in Fig. 13.

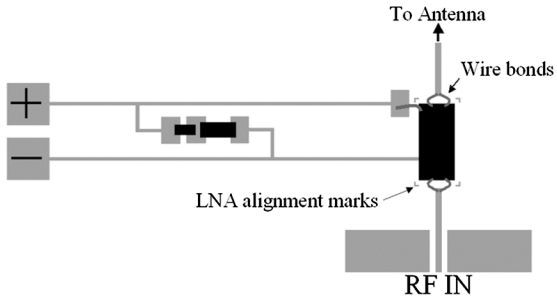

Fig. 12. LNA was integrated by centering it between the corner alignment marks. Five wire bonds were added to connect the LNA to the dc bias and to the RF signal lines.

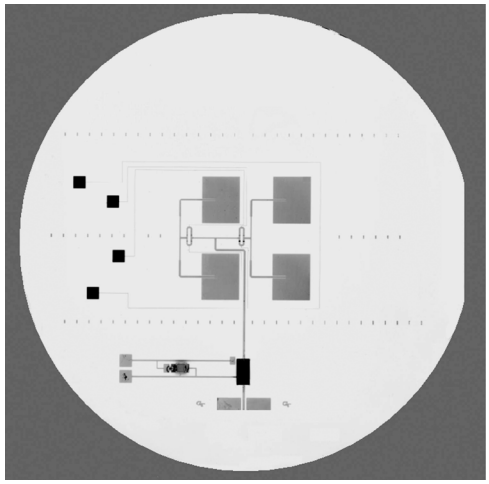

Fig. 13. Fabricated single-layer antenna array is shown. The parts were labeled in Fig. 11.

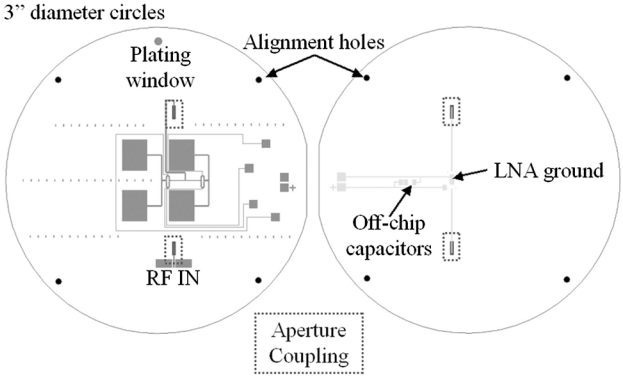

Fig. 14. Layout of multilayer antenna array. The 2 × 2 patch antenna array, MEMS phase shifters, bias lines, and LNA pads are shown.

B. Multilayer System-On-Package

Implementing the multilayer configuration is much more challenging than the single-layer configuration because this approach requires multisubstrate alignment, device packaging, substrate bonding, fabrication on two sides of a substrate, and a method for transmitting the data across layers.

The final layout for the multilayer antenna array is shown in Fig. 14. The device operates just like the single-layer device except the signal is transmitted to a lower layer and back to the

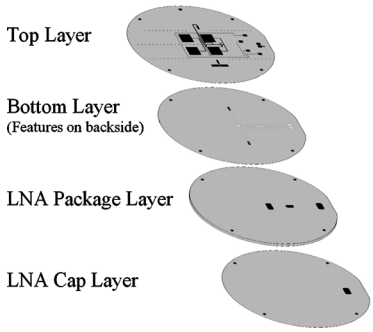

Fig. 15. Stack-up of multilayer antenna array. The features shown on the bottom layer are actually on the backside. The cavities in the LNA package layer line up to protect the chip, wire bonds, capacitors, and to open a window for dc probing.

top layer by aperture coupling. The LNA was centered directly under the 2×2 array.

The substrate material was cut into the same size and shape as the previous implementation. The notch on the side of the wafer was particularly useful in this design because it is easy to get the samples turned around when fabricating on the top and bottom side of a substrate. To aid in the alignment of the substrate layers, four 1/16th inch (1.5875 mm) diameter holes were laser cut in the corners of the substrate. Steel pins of the same size were used to align the layers during bonding and were removed directly after. The alignment accuracy for this method is estimated to be within 50 μm.

The top substrate (left side of Fig. 14) was fabricated in the same way as the single-layer approach without the LNA. On the backside of the top substrate, the metal layer is etched to provide the window for aperture coupling. This is done by patterning with photoresist and etching using nitric acid. Backside alignment is possible within 5–10 μm.

The bottom substrate (right side of Fig. 14) has its features fabricated on the backside on the substrate (notice the notch is now on the left).

The final fabrication stack-up is shown in Fig. 15. There are four main layers. The top layer has the RF input, MEMS phase shifters, and phased array. The bottom layer has the LNA and off-chip capacitors. The LNA package layer has laser micromachined cavities which protect the LNA, wire bonds, and off-chip capacitors. It also provides a window for accessing the LNA dc bias pads. The LNA cap layer covers the cavities to protect the components inside. The dc bias for the LNA is accessed on the back side of the antenna to minimize interference of the dc biasing wires with the antenna. If desired, they can be brought to the top layer for probing with a bond wire or metalized via hole.

Before the system is assembled, all of the layers are fabricated independently and then bonded together. There are three popular methods for bonding LCP: thermocompression, localized ring [14], and epoxy [1]. Unfortunately, none of these methods could be exclusively used to bond the layers. The MEMS switches and LNA cannot survive the thermocompression bonding temperature ($\sim$290°C) [10]. Localized ring bonding cannot penetrate through the 1.3 mm thick LNA package layer [14]. Epoxy bonding over 20 layers would be very messy and difficult to control. Therefore, a combination

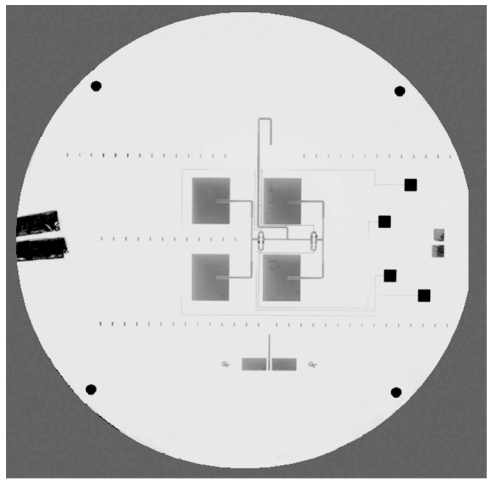

(a)

Fig. 16. Fabricated multilayer antenna array is shown. The parts were labeled in Fig. 14.

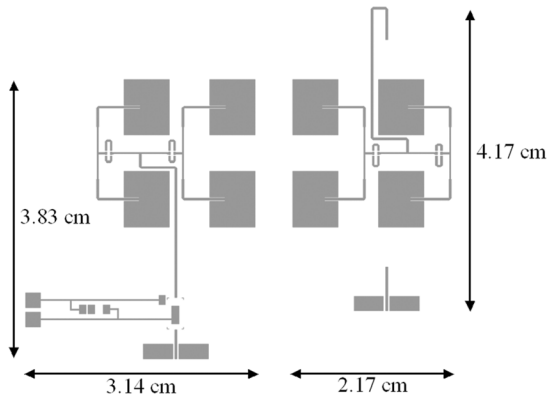

Fig. 17. Size of the two implementations is shown to scale. The multilayer configuration (on the right) is 25% smaller than the single-layer configuration (on the left).

of techniques was used. To bond the thick LNA package layer, thermocompression bonding was used. The top and bottom layers were bonded using epoxy bonding since it has been proven to be an easy, low-loss packaging method [1]. The LNA cap layer was also bonded using epoxy.

The fabricated multilayer SOP antenna array is shown in Fig. 16.

C. Comparison of Technologies

The single and multilayer implementations both perform the same function (beam steering at 14 GHz). However, there are three main differences: size, loss, and degree of expandability.

1) Size Comparison: For both implementations, the phase shifters, LNA, and 2×2 antenna array are identical. The size difference comes from the LNA being on a different layer and centered under the 2×2 antenna array, some of the RF distribution network being on a different layer, and the dc bias lines for the LNA being on a different layer. The size of the two implementations is compared in Fig. 17.

The multilayer configuration is 25% smaller by moving the LNA to a lower layer. Since these designs were intended to serve as a prototype, the antenna arrays were made as small as possible while maintaining proper distance between components to

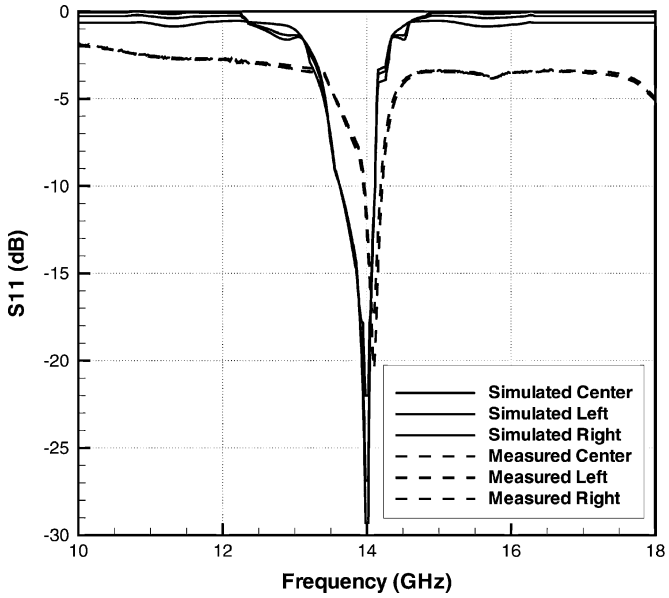

Fig. 18. Measured hard-wired passive antenna array return loss is compared to the simulation results. The results show good agreement.

reduce coupling. Each design could be made smaller by using metal-filled vias instead of aperture coupled vias.

2) Loss Comparison: The multilayer configuration is inherently lossier than the single-layer because it has a longer RF signal length and uses aperture coupling. The line loss can be minimized by using thick, highly conductive metal. The aperture coupling loss can be minimized by properly simulating the device and having good alignment accuracy during fabrication. The use of metal-filled vias would also reduce the loss.

3) Degree of Expandability: As more components and functionality are added to the systems, the size will inherently grow. In the single-layer case, this means a larger area. For the multilayer case, the area can be kept constant and the thickness can increase. Adding an additional layer of RF components increases the thickness of the SOP by a few hundred microns but adds another 30.4 square centimeters of area. A lot of additional functionality can be added within this area.

Another advantage to the multilayer implementation is that the antenna is shielded from the other components in the system. The metal ground plane below the patch antennas is capable of preventing radiation from the other system components from effecting the radiation pattern. This is not the case with the single-layer implementation.

V. Antenna Array Testing and Results

Before the complete phased array antenna is characterized, the antenna array with hard-wire switches and the LNA are measured. This is to verify that the components and system were operating as expected.

A. Passive Antenna Array Return Loss Measurements

The 2×2 antenna array with hard-wired phase shifters was measured using 800 μm pitch GSG RF probes. TRL calibration was performed to remove the cable and connector losses. The measured results are shown in Fig. 18.

TABLE IV
Resonant Frequency and 10 dB Return Loss Bandwidth of the Simulated and Measured Passive Antenna Array With Hard-Wire Switches

	$f_{Resonant}$	10 dB Return Loss BW	Percent BW
Simulated Left	14.00GHz	487MHz	3.48%
Measured Left	14.10GHz	248MHz	1.76%
Simulated Center	14.00GHz	489MHz	3.49%
Measured Center	14.05GHz	240MHz	1.71%
Simulated Right	14.00GHz	488MHz	3.49%
Measured Right	14.10GHz	245MHz	1.74%

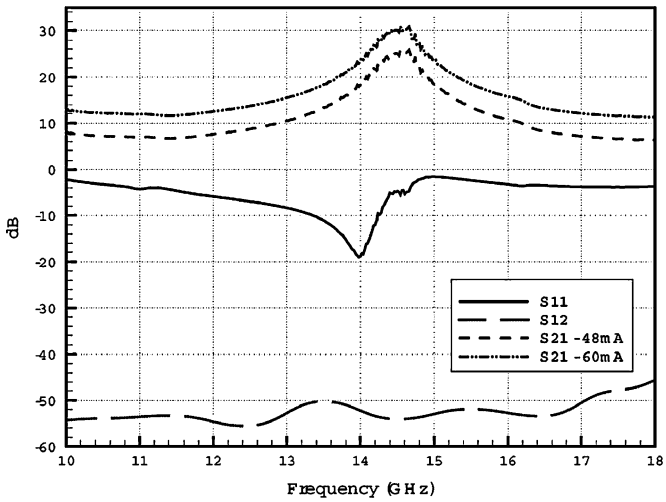

Fig. 19. The measured performance of the LNA mounted to an LCP sample is shown. The gain increases with the bias current. The S11 and S12 do not change with different loads on the output port. These measurements include the loss from the wire bonds.

The resonant frequency and 10 dB return loss bandwidth are given in Table IV. There is good agreement between the simulated and measured data. Having a bandwidth of a few percent is common with these type of antennas [15].

B. LNA Measurement Results

The LNA was mounted to an LCP sample using the same setup as with the antenna arrays. The measured performance of the LNA by itself on LCP is shown in Fig. 19. The gain for two different bias currents is shown. A higher bias current results in a higher gain. The measured return loss and gain at 14 GHz are 19 dB and 23 dB, respectively for a 60 mA bias current. The S12 is less than -50 dB across the band.

C. Pattern Measurement Setup

An RF probe station, far field antenna range measurement was performed. During the test, the antenna under test is positioned on a piece of Styrofoam and fed by an 800 micron pitch GSG RF probe. The array antenna is fed by a 14 GHz signal and the receiving antenna sweeps in a 360 degree arc around the antenna under test. The input RF power is monitored throughout the test by an RF power meter, and the power at the receiving antenna is measured with a crystal detector and lock-in amplifier. Two dc probe positioners are used to apply the actuation voltage to each phase shifter (the switches were grounded by a floating

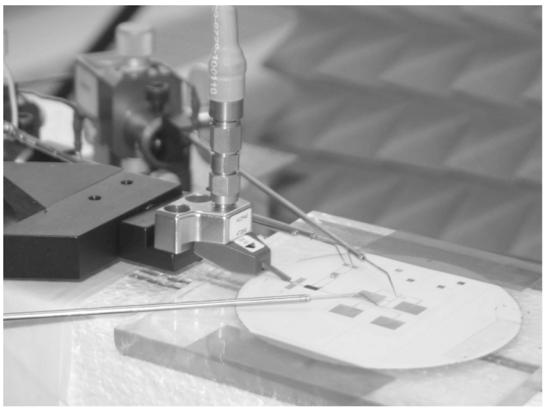

(a)

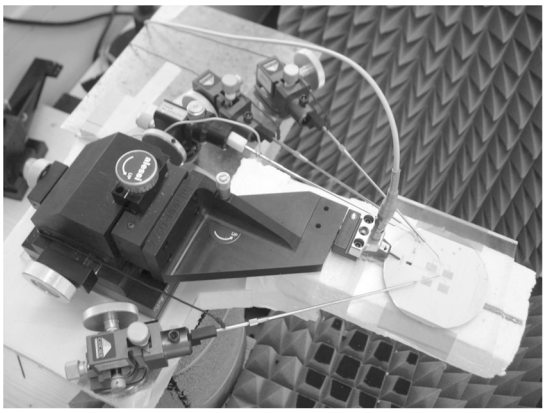

(b)

Fig. 20. Radiation pattern measurement setup is shown. This setup applies to the single and multilayer SOP. (a) Sample is shown with four dc probes and the RF probe. (b) Setup is shown from above.

ground). For the single-layer SOP, two additional dc probe positioners were used to apply the 2 V bias voltage and ground to the LNA, while for the multilayer SOP, the LNA dc bias was applied to the back of the package. These probes caused some noise and a small dimple to appear in the pattern. A collection of measurement images is shown in Fig. 20.

Microcracks in the high impedance bias lines prevented biasing from the dc probe pads. Instead, the biasing was applied directly to the feed network. This can be seen in Fig. 20(a).

D. Single-Layer SOP Measurements

Since the single-layer antenna array is very thin, it was mounted to a glass plate using spray epoxy before measuring. The glass plate was under the metal ground plane so it should have a negligible effect on the radiation pattern. This was shown in Fig. 20(a).

1) Return Loss Measurements: Because S12 of the LNA is small, the return loss of the antenna array is set by the return loss of the LNA. This helps to isolate the return loss of the array from variations in return loss of the phase shifters during switching. The measured return loss of the antenna array is shown in Fig. 21. There is only one plot since the state of the phase shifters has a negligible effect on the return loss. For comparison, the return loss of the LNA is also shown on Fig. 21.

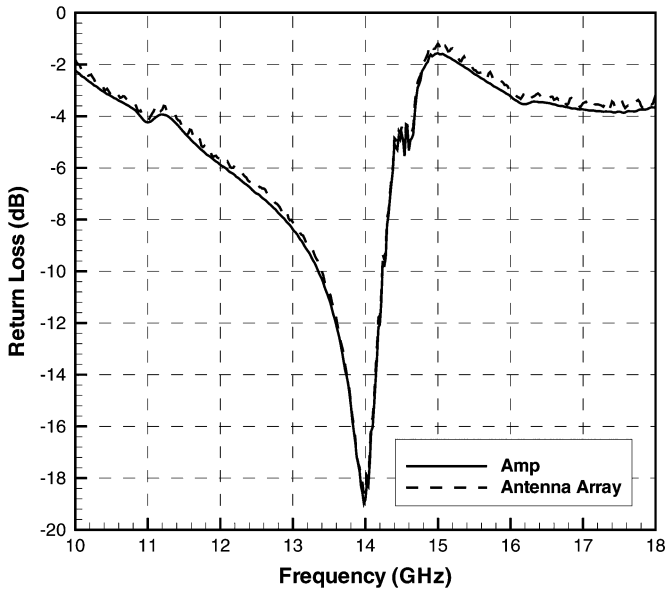

Fig. 21. Measured return loss for the single-layer antenna array and the LNA.

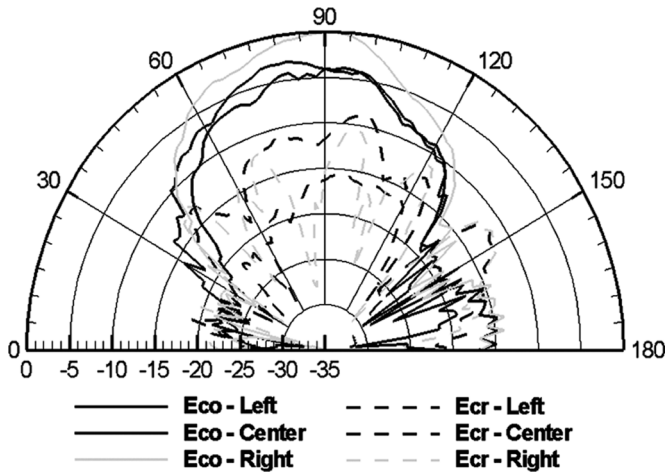

Fig. 22. Measured E-plane co-pol and cross-pol are compared for the single-layer antenna array. The data has been normalized.

2) Radiation Pattern Measurements: The measured E-plane co-pol and cross-pol results are shown in Fig. 22. The cross-pol level is more than 10 dB lower than the co-pol level over most of the half-space. It was expected that the cross-pol level would be higher than desired due to the measurement setup. From the images in Fig. 20, many sources of scattering can be found. Some of the largest contributors to the high cross-pol are the dc probes, the probe positioners, and the large steel plate that the dc probes are mounted to.

The raw data was normalized and smoothed using a MATLAB 3rd order moving average filter to remove some of the noise in the pattern. These results are shown in Fig. 23. The beam is able to sweep from -8° to $+4^\circ$. These results agree well with the simulated results which predicted a sweep from -9° to $+6^\circ$. The shape of the beam matches well with the ones shown in Fig. 9.

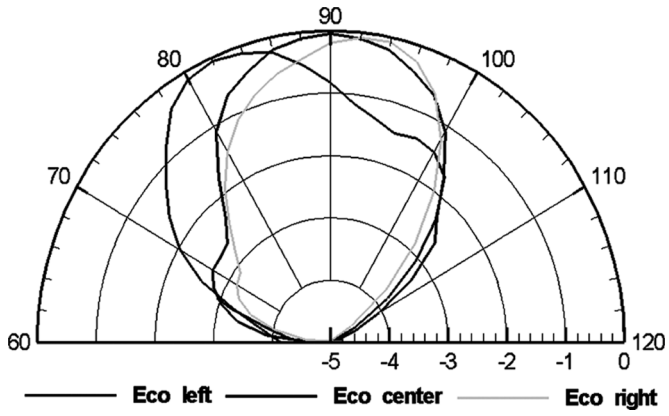

Fig. 23. Degree of beam steering for the single-layer antenna array is emphasized. The measurements have been filtered to remove the noise. The beam can be steered left by 8° and right by 4°. The beam is centered perpendicular to the antenna. The data has been normalized.

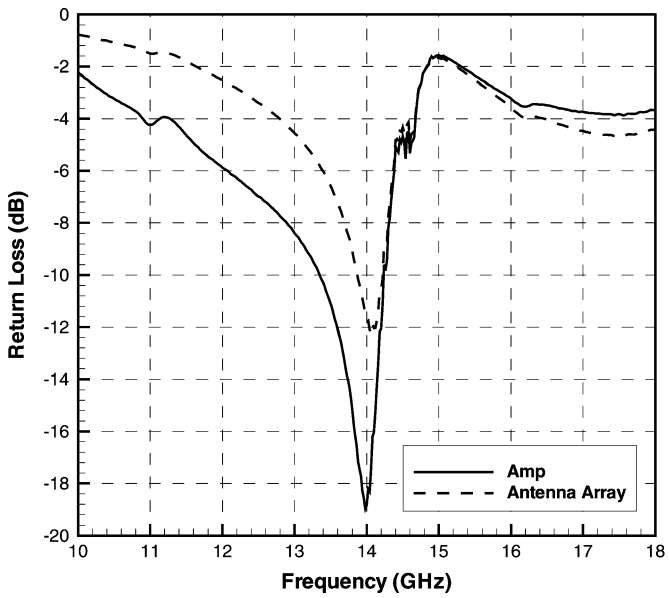

Fig. 24. Measured return loss for the multilayer antenna array and LNA.

E. Multilayer SOP Measurements

Unlike the single-layer antenna array, the multilayer device is more rigid and does not need to be mounted onto the glass plate. The antenna array was measured in the same fashion as the single-layer device.

1) Return Loss Measurements: Unlike the single-layer SOP, this implementation will not have a return loss identical to the LNA since the LNA is after the first coupling aperture. However, if the aperture coupling is properly designed, the return loss of the LNA and the antenna array should be very similar. The measured return loss of the antenna array is shown in Fig. 24 with the return loss of the LNA. The return loss of the LNA and the antenna array are similar, which indicates that the aperture coupling design is good.

2) Radiation Pattern Measurements: The measured E-plane co-pol results were normalized and smoothed using a MATLAB 5th order moving average filter to remove most of the noise in the pattern. These results are shown in Fig. 25 and the beam steering is emphasized in Fig. 26. The beam is able to sweep from -4° to $+8^\circ$.

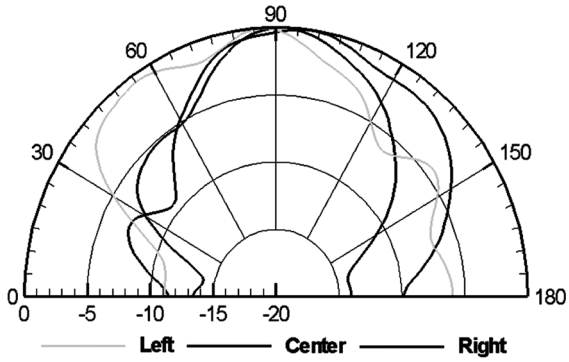

Fig. 25. Measured E-plane co-pol for the multilayer antenna array. The filtered data was calculated using a 5th order moving average filter in MATLAB. The data has been normalized.

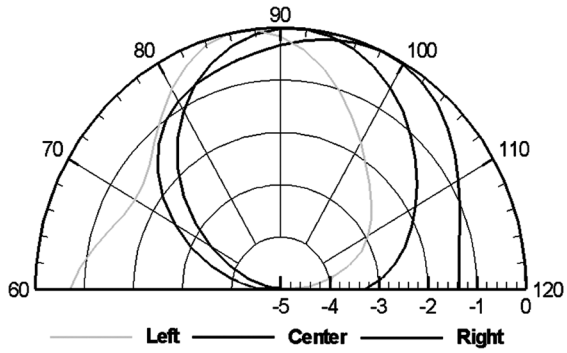

Fig. 26. Degree of beam steering is emphasized for the multilayer antenna array. The beam can be steered left by 4° and right by 8°. The data has been normalized.

F. Measured Gain of Passive Antenna Array

The gain of an antenna is not related to the input power. It almost seems counter intuitive, but adding an LNA to an antenna does not change the gain of the antenna array that is defined as the phase shifters and antenna elements. Instead, it increases the power radiated so that a lower input power can be used or the antenna can transmit further.

The antenna array gain was measured using a comparative method. The raw pattern data was compared to the measured data for a 10 dBi gain horn antenna, with the power level adjusted so that the gain horn received the same amount of input power as the 2×2 antenna array.

The procedure for calculating the gain is described in Table V. The calculated and simulated values both agree that the gain is approximately 7.75 dB. The simulated value matches closely to the measured value because the substrate and metal losses were included in the simulation.

G. Single-Layer SOP Loss Analysis

The simulated directivity for this antenna array using ADS Momentum is 12.58 dB, which is expected for a four element array. Since the measured gain was 7.75 dB, this calculates to an estimated 4.83 dB of loss for the antenna array. Most of the loss comes from substrate and metal losses. This was demonstrated

TABLE V
GAIN CALCULATION FOR THE PASSIVE ANTENNA ARRAY. VALUES ARE TAKEN IN THE DIRECTION OF MAXIMUM RADIATION. SIMULATED AND MEASURED VALUES AGREE VERY WELL

Antenna Parameter	Value
Measured power for single-layer SOP	-43.97 dB
Measured power for gain horn	-41.72 dB
Difference in measured power	-41.72 – -43.97 = 2.25 dB
Measured gain	10 – 2.25 = 7.75 dB
Simulated gain with MEMS switches	7.5 dB
Simulator discrepancy	0.25 dB (3.2%)

in the previous section since the simulated (with substrate and metal losses) and measured gains were nearly identical.

The measured loss of a transmission line on 100 μm thick LCP is 0.375 dB/cm. The total feed network length is 10.04 cm. This gives a line loss of 3.77 dB. Of that, 0.34 dB is from the phase shifters. There is an additional 0.20 dB of loss from each MEMS switch. Since there are four switches activated at any given time, that equates to 0.80 dB of added loss. In total, there are 4.57 dB of loss from the MEMS and line length. There is 0.36 dB of additional loss that is unaccountable, which is a minimal margin of error.

H. Multilayer SOP Loss Analysis

As stated before, there are a few sources of additional loss in the multilayer implementation that were not present in the single-layer approach. This is going to reduce the amount of power radiated from the phased array antenna.

The multilayer SOP has 3.54 cm of additional line length than the single-layer module because the feed network traverses under the antenna array as shown in Fig. 14(b). At 0.375 dB/cm, this equates to an additional 1.33 dB of line loss.

Each aperture coupling will result in power reflected from impedance mismatch and an insertion loss from radiation and epoxy. It was shown in Fig. 24 that the first aperture caused the return loss of the antenna array to decrease from 19 dB to 12 dB (an additional 5% power reflected). This additional loss is minimal, but it could be further reduced by using metal-filled vias.

I. Analysis of Beam Steering

The single-layer antenna array is capable of steering left by 8° and right by 4°. The multilayer antenna array is capable of steering left by 4° and right by 8°. The directions "left" and "right" are given with respect to the RF probe feed. Therefore, the multilayer antenna is fed in the opposite direction as the single-layer antenna. This can be seen in Fig. 17. The amount of beam steering is the same whether we use a single or multilayer implementation.

The desired amount of beam steering varies by the application. Changing the phase shift between patches will change the degree of beam steering. For this antenna array geometry, if the phase shift was increased to 180°, the beam could be steered $\pm 42°$. Adding more patches to the antenna will result in a higher degree of beam steering. Adding a multibit phase shifter would give more resolution to the beam. For example, integrating a 4-bit 180° phase shifter into this antenna array would provide 16 different beam angles between $-42°$ and 42°.

Patch antenna arrays are sensitive to flexing but LCP is not. Antenna arrays that are mounted to a curved surface are certainly possible, but the curvature must be designed into the array. The array used in this paper is intended for flat operation. Temporary flexing for transportation is not a problem.

VI. CONCLUSION

For the first time, a fully integrated phased antenna array on a flexible, organic substrate has been demonstrated. LCP was used as both the RF substrate and packaging material. By integrating MEMS switches into a patch antenna array, it was possible to steer a beam by a total of 12°. MEMS switches were used to keep the losses to a minimum. The use of an LNA allowed for a much higher radiated power level.

Both single and multilayer implementations were investigated and compared. Overall, the simulated and measured results agreed very well.

This research demonstrates the first complete system on a flexible, organic polymer. It is small, low-cost, low-loss, flexible (for the single-layer device), and capable of beam steering. These devices can be customized to meet almost any size, frequency, and performance needed. This research furthers the state-of-the-art for organic SOP devices.

ACKNOWLEDGMENT

The authors would like to thank L. Rose, with the Georgia Tech Microelectronics Research Center, for assisting with the wire bonding.

REFERENCES

[1] N. Kingsley and J. Papapolymerou, "Organic 'wafer-scale' packaged miniature four-bit RF MEMS phase shifter," *IEEE Trans. Microw. Theory Tech.*, vol. 54, no. 3, Mar. 2006.

[2] L. Whicker, "Active phased array technology using coplanar packaging technology," *Trans. Antennas Propag.*, vol. 43, no. 9, pp. 949–952, Sep. 1995.

[3] Y. Mancuso, P. Gremillet, and P. Lacomme, "T/R-modules technological and technical trends for phased array antennas," in *IEEE MTT-S Int. Microwave Symp. Digest*, Jun. 2006, pp. 614–617.

[4] R. Tummala, "SOP: what is it and why? a new microsystem-integration technology paradigm—Moores law for system integration of miniaturized convergent systems of the next decade," *IEEE Trans. Adv. Packag.*, vol. 27, pp. 241–249, May 2004.

[5] M. K. Iyer, P. V. Ramana, K. Sudharsanam, C. J. Leo, M. Sivakumar, B. Pong, and X. Ling, "Design and development of optoelectronic mixed signal system-on-package (SOP)," *IEEE Trans. Adv. Packag.*, vol. 27, no. 2, pp. 278–285, May 2004.

[6] L. Jong-Hoon, G. DeJean, S. Sarkar, S. Pinel, L. Kyutae, J. Papapolymerou, J. Laskar, and M. M. Tentzeris, "Highly integrated millimeter-wave passive components using 3-D LTCC system-on-package (SOP) technology," *IEEE Trans. Microw. Theory Tech.*, vol. 53, no. 6, pt. II, pp. 2220–2229, Jun. 2005.

[7] C. Lugo and J. Papapolymerou, "Electronic switchable bandpass filter using PIN diodes for wireless low cost system-on-a-package applications," *Proc. Inst. Elect. Eng. Microwaves, Antennas and Propagation*, vol. 151, no. 6, pp. 497–502, Dec. 2004.

[8] K.-I. Shinotani, P. M. Raj, M. Seo, S. Bansal, H. Sakurai, S. K. Bhattacharya, and R. Tummala, "Evaluation of alternative materials for system-on-package (SOP) substrates components and packaging technologies," *IEEE Trans. Compon., Packag. Man. Technol., Part A: Packag. Technol.*, vol. 27, no. 4, pp. 694–701, Dec. 2004.

[9] D. Thompson, O. Tantot, H. Jallageas, G. Ponchak, M. Tentzeris, and J. Papapolymerou, "Characterization of liquid crystal polymer (LCP) material and transmission lines on LCP substrates from 30 to 110 GHz," *IEEE Trans. Microw. Theory Tech.*, vol. 52, pp. 1343–1352, Apr. 2004.

[10] N. D. Kingsley, "Development of miniature, multilayer, integrated, reconfigurable RF MEMS communication module on liquid crystal polymer (LCP) substrate," Ph.D. dissertation, Georgia Tech., Atlanta, GA, 2007.

[11] C. Balanis, *Antenna Theory: Analysis and Design*, 2nd ed. New York: Wiley, 1982.

[12] Z. Aboush, J. Benedikt, J. Priday, and P. J. Tasker, "DC-50 GHz low loss thermally enhanced low cost LCP package process utilizing micro via technology," in *IEEE MTT-S Int. Microwave Symp. Digest*, Jun. 2006, pp. 961–964.

[13] D. Pozar, "A review of aperture coupled microstrip antennas: history, operation, development, and applications," *Lecture Note* May 1996 [Online]. Available: http://www.ecs.umass.edu/ece/pozar/aperure.pdf

[14] M. Morton, N. Kingsley, and J. Papapolymerou, "Low cost method for localized packaging of temperature sensitive capacitive RF MEMS switches in liquid crystal polymer," in *IEEE MTT-S Int. Microwave Symp.*, Honolulu, HI, Jun. 2007, pp. 2075–2078.

[15] G. DeJean, R. Bairavasubramanian, D. Thompson, G. Ponchak, M. Tentzeris, and J. Papapolymerou, "Liquid crystal polymer (LCP): a new organic material for the development of multilayer dual-frequency/dual-polarization flexible antenna arrays," *Antennas Wireless Propag.*, no. 4, pp. 22–26, 2005.

Nickolas Kingsley (S'02–M'07) received B.S., M.S., and Ph.D. degrees in electrical engineering from the Georgia Institute of Technology (Georgia Tech), Atlanta, in 2002, 2004, and 2007 respectively.

He was a member of the Georgia Electronic Design Center (GEDC), Georgia Tech, under the direction of Prof. John Papapolymerou until May 2007. In June 2007, he joined Auriga Measurement Systems, Lowell, MA as a Principal Engineer. He will be developing high performance amplifier systems and RF assemblies. His research interests focused on developing miniature, multilayer, system-on-package (SOP) RF front ends using liquid crystal polymer (LCP) substrate. During his thesis work, he investigated methods for packaging RF MEMS switches in flexible, organic packages and tested for reliability. He has published one book chapter and over a dozen publications and has submitted four invention disclosures.

Dr. Kingsley won numerous awards while at Georgia Tech. He is the recipient of the 2002 President's Undergraduate Research Award. He won three poster competitions at the university, college, and school levels. He earned the Trainer of the Year distinction from the Microelectronics Research Center Cleanroom in 2005 and 2006. As a coop student with Compaq Computer Corporation, he won the 2001 Armada Award for excellence. He is a member of the IEEE APS, IEEE MTT-S, and Order of the Engineer. He will serve as a TPC member for the 2008 IMS conference in Atlanta, GA.

George E. Ponchak (S'82–M'83–SM'97) received the B.E.E. degree from Cleveland State University, Cleveland, OH, in 1983, the M.S.E.E. degree from Case Western Reserve University, Cleveland, OH, in 1987, and the Ph.D. in electrical engineering from the University of Michigan, Ann Arbor, in 1997.

He joined the staff of the Communication Technology Division, NASA Glenn Research Center, Cleveland, OH, in 1983 where he is now a Senior Research Engineer. In 1997–1998 and in 2000–2001, he was a Visiting Lecturer at Case Western Reserve University. He has authored and coauthored over 140 papers in refereed journals and symposia proceedings. His research interests include the development and characterization of microwave and millimeter-wave printed transmission lines and passive circuits, multilayer interconnects, uniplanar circuits, Si and SiC radio frequency integrated circuits, and microwave packaging.

Dr. Ponchak is an Associate Member of the European Microwave Association. He is Editor-in-Chief of the IEEE MICROWAVE AND WIRELESS COMPONENTS LETTERS, and he was Guest Editor of a special issue of the IEEE TRANSACTIONS MICROWAVE THEORY AND TECHNIQUES on Si MMICs. He founded the IEEE Topical Meeting on Silicon Monolithic Integrated Circuits in RF Systems and served as its Chair in 1998, 2001, and 2006. He served as Chair of the Cleveland MTT-S/AP-S Chapter (2004–2006), and he has chaired many MTT-S International Microwave Symposium workshops and special sessions. He is a member of the IEEE International Microwave Symposium Technical Program Committee on Transmission Line Elements and served as its Chair in 2003–2005, a member of IEEE MTT-S AdCom Membership Services Committee (2003–2005), and a member of the IEEE MTT-S Technical Committee 12 on Microwave and Millimeter-Wave Packaging and Manufacturing. He received the Best Paper of the ISHM'97 30th International Symposium on Microelectronics Award.

John Papapolymerou (S'90–M'99–SM'04) received the B.S.E.E. degree from the National Technical University of Athens, Athens, Greece, in 1993, and the M.S.E.E. and Ph.D. degrees from the University of Michigan, Ann Arbor, in 1994 and 1999, respectively.

From 1999 to 2001, he was an Assistant Professor at the Department of Electrical and Computer Engineering, University of Arizona, Tucson, and during summers 2000 and 2003, he was a Visiting Professor at the University of Limoges, France. From 2001 to 2005, he was an Assistant Professor at the School of Electrical and Computer Engineering, Georgia Institute of Technology, where he is currently an Associate Professor. He has authored or coauthored over 140 publications in peer reviewed journals and conferences. His research interests include the implementation of micromachining techniques and MEMS devices in microwave, millimeter-wave and THz circuits and the development of both passive and active planar circuits on semiconductor (Si/SiGe, GaAs) and organic substrates (LCP, LTCC) for system-on-a-chip (SOC)/system-on-a-package (SOP) RF front ends.

Dr. Papapolymerou received the 2004 Army Research Office (ARO) Young Investigator Award, the 2002 National Science Foundation (NSF) CAREER award, the best paper award at the 3rd IEEE International Conference on Microwave and Millimeter-Wave Technology (ICMMT2002), Beijing, China and the 1997 Outstanding Graduate Student Instructional Assistant Award presented by the American Society for Engineering Education (ASEE), The University of Michigan Chapter. His student also received the best student paper award at the 2004 IEEE Topical Meeting on Silicon Monolithic Integrated Circuits in RF Systems, Atlanta, GA. He currently serves as the Vice-Chair for Commission D of the US National Committee of URSI and as an Associate Editor for the IEEE MICROWAVE AND WIRELESS COMPONENT LETTERS and the IEEE TRANSACTIONS ON ANTENNAS AND PROPAGATION. During 2004 he was the Chair of the IEEE MTT/AP Atlanta Chapter.